

Supported Pt Enabled Proton-Driven NAD(P)⁺ Regeneration for Biocatalytic Oxidation

Joseph W.H. Burnett,^{1,2,†} Hui Chen,^{3,†} Jianwei Li,¹ Ying Li,⁴ Shouying
Huang,⁴ Jiafu Shi,⁵ Alan J. McCue,⁶ Russell F. Howe,⁶ Shelley D.
Minteer^{3,*} and Xiaodong Wang^{1,*}

¹Chemical Engineering, Department of Engineering, Lancaster University, Lancaster
LA1 4YW, United Kingdom

²Chemical and Materials Engineering, School of Engineering, University of Aberdeen,
Aberdeen AB24 3UE, United Kingdom

³Department of Chemistry, University of Utah, Salt Lake City, Utah 84112, United
States

⁴School of Chemical Engineering and Technology, Tianjin University, Tianjin 30072,
China

⁵School of Environmental Science and Engineering, Tianjin University, Tianjin 300072,
China

⁶Department of Chemistry, University of Aberdeen, Aberdeen AB24 3UE, United
Kingdom

Corresponding author E-mail:

S.D.M.: minteer@chem.utah.edu; X.W.: xiaodong.wang@lancaster.ac.uk

[†]These authors contributed equally to this work.

Abstract

The utilisation of biocatalytic oxidations has evolved from the niche applications of the early 21st century to a widely recognised tool for general chemical synthesis. One of the major drawbacks that hinders commercialisation is the dependence on expensive nicotinamide adenine dinucleotide (NAD(P)⁺) cofactors and so their regeneration is essential. Here, we report the design of carbon-supported Pt catalysts that can regenerate NAD(P)⁺ by proton-driven NAD(P)H oxidation with concurrent hydrogen formation. The carbon support was modified to tune the electronic nature of the Pt nanoparticles and it was found that the best catalyst for NAD(P)⁺ regeneration (TOF = 581 h⁻¹) was electron rich Pt on carbon. Finally, the heterogeneous Pt catalyst was applied in the biocatalytic oxidation of a variety of alcohols catalysed by different alcohol dehydrogenases. The Pt catalyst exhibited good compatibility with the biocatalytic system. Its NAD(P)⁺ regeneration function successfully supported biocatalytic conversion from alcohols to corresponding ketone or lactone products. This work provides a promising strategy for chemical synthesis via NAD(P)⁺-dependent pathways, utilising a cooperative inorganic-enzymatic catalytic system.

Keywords: NAD(P)⁺ regeneration, biocatalytic oxidation, dehydrogenase, heterogenous Pt catalysis, hydrogen.

Introduction

Enzymes are capable of performing complex biotransformations under environmentally benign reaction conditions with unparalleled specificity.¹⁻⁴ To retain these advantages and combine them with the reactivity and durability of artificial systems, the field of cooperative catalysis has become increasingly popular.⁵ Cooperative catalysis involving at least one biological enzyme has exhibited promising performance in asymmetric reductions, reductive aminations, dynamic kinetic resolution, hydrolysis and reduction.⁶⁻⁸ A representative cooperative system are enzymatic reactions that consume cofactors and are coupled to a second catalyst used to regenerate the cofactor. NAD(P)-dependent oxidoreductases catalyse a diverse range of industrially significant reactions, including the oxidation of alcohols, aldehydes and carboxylic acids with applications in pharmaceutical, fine and bulk chemical sectors.^{9,10} Despite their significance, the industrial application is constrained by the stoichiometric consumption of the expensive cofactor NAD(P)⁺ (prices¹¹: \$1400 per mole NAD⁺ and \$18000 per mole of NADP⁺).⁹ To overcome this, the *in situ* oxidation of NAD(P)H back to NAD(P)⁺ (i.e., NAD(P)⁺ regeneration, see [Figure 1a](#)) is essential.¹²

NAD(P)⁺ regeneration has so far been reported utilising enzymatic (e.g., NADH oxidase), homogeneous (e.g., organic metal complexes), photocatalytic (e.g., photoexcited flavin), electrocatalytic (e.g., redox mediators) and very recently heterogeneous (e.g., Au/oxide) catalytic systems.¹³⁻¹⁶ The majority of the reported regeneration systems have taken inspiration from NADH oxidases or NADH dehydrogenases, which are enzymes that can oxidise NAD(P)H to NAD(P)⁺ using molecular O₂ as an oxidant, forming H₂O or H₂O₂ in the process (e.g., the Au/oxide system¹³).¹⁷⁻²⁰ Another approach is inspired by (NAD(H)-linked) hydrogenases, which

is preferred as it is only dependent on readily available protons (coming from the substrate in an actual enzymatic oxidation reaction), does not require O₂ or form H₂O₂ (both of which enzymes are frequently intolerant to) and generates H₂ as a green energy product that can be easily removed, shifting the equilibrium in favour of both regeneration and ultimately the biocatalytic reactions.²¹ However, it is a substantial chemical challenge due to the much weaker oxidising capacity of H⁺. Successful cooperative methods that have facilitated proton-driven NADH oxidation often require expensive and complex enzymatic systems or a supply of extra solar/electrical energy, as shown in [Figure 1b-d](#).²²⁻²⁵ Organometallic systems (e.g., [Figure 1e](#)) are exceptions to this; however, due to the often observed mutual deactivation (between the catalyst and the enzyme), more complex downstream separation and sometimes acidic operational conditions, it is unlikely that these are strong candidates for scale-up.^{26,27}

Heterogeneous catalysis is a form of synthetic catalysis that is directly involved in the production of 90% of chemicals globally.²⁸ Due to its heterogeneous nature, the catalyst is easily removed from liquid/gas phases, enhancing product separation and has the potential for catalyst recycling, reuse and ease of scale-up. In this work, we demonstrate that heterogeneous catalysts (Pt/C) can promote proton-driven oxidation of NAD(P)H for selective NAD(P)⁺ regeneration with concurrent H₂ formation (see [Figure 1f](#)), functionally acting as (NAD(H)-linked) hydrogenases. The catalytic activity can be tuned by modifying the carbon support and altering the Pt electronic structure. The Pt/C catalysts are compatible with biocatalytic systems and can be used to support a range of biocatalytic alcohol oxidations via *in situ* cofactor regeneration. Cooperative heterogeneous-enzymatic catalysis offers significant downstream separation advantages and provides a general strategy for chemical synthesis by NAD(P)⁺-dependent enzymes.

Experimental

Materials.

β -Nicotinamide adenine dinucleotide reduced disodium salt hydrate ($\geq 94\%$), β -nicotinamide adenine dinucleotide hydrate ($\geq 96.5\%$), β -Nicotinamide adenine dinucleotide 2'-phosphate reduced tetrasodium salt hydrate ($\geq 97\%$), β -Nicotinamide adenine dinucleotide phosphate hydrate ($\geq 95\%$), potassium phosphate dibasic trihydrate ($\geq 99\%$), potassium phosphate monobasic ($\geq 99\%$), potassium hydroxide (90%) hexachloroplatinic acid solution (8% w/w in water), hydrogen peroxide (30% w/w), diphenylamine (99%), dihydroxyacetone ($\geq 98\%$), 1-heptanol (98%), heptanal ($>95\%$), (S)-(+)-2-octanol, 2-octanone (98%), (S)-(-)-1-phenylethanol, acetophenone, 1,5-pentanediol (96%), and δ -Valerolactone were supplied by Sigma Aldrich. Activated charcoal (untreated, granular, 4-8 mesh), sulfuric acid (95%), acetic acid (99.7% w/w) and hydrochloric acid (36.5-38.0%) were purchased from Fisher Scientific. The nitrogen and oxygen gases of ultrahigh purity ($\geq 99.99\%$) were supplied by BOC. EnzyChrom™ NADH/NAD⁺ cycling assay kit was purchased from Universal Biologicals.

The genes of alcohol dehydrogenase variant from *Thermoanaerobacter ethanolicus* (TesADH, W110A/G198D, Genbank: WP_041589967.1), (S)-Specific 1-phenylethanol dehydrogenase of the denitrifying *Bacterium* Strain EbN1 (AA-ADH, PDB: 2EW8), and alcohol dehydrogenase E chain of horse (HL-ADH, Uniport: P00327) were synthesized by GenScript Biotech Corp. and inserted into pET-28a plasmid with a N-terminal histidine tag. The gene of alcohol dehydrogenase from *Geobacillus stearothermophilus* (ADH-hT, Uniport: P42328) was synthesized by GenScript Biotech Corp. and inserted into pET20a plasmid with a C-terminal histidine tag. The molecular

weight of TesADH, AA-ADH, HL-ADH, and ADH-hT is 40kDa, 29kDa, 42kDa, and 37kDa, respectively.

Catalyst Preparation and Characterisation.

Activated charcoal was used as the starting material for all carbon samples. Before post-treatments, the activated charcoal was washed by refluxing in H₂O for 24 h, filtered, and dried at 383 K for 24 h. This untreated carbon carrier was referred to as C-1. For the liquid phase treated carbons, C-1 was refluxed in either 5 M or 10 M of HNO₃ (referred to as C-2 and C-3, respectively) or 10 M H₂O₂ (C-4) for 24 h. The carbons were then filtered, washed with H₂O until the effluent achieved a neutral pH then dried at 383 K for 24 h. Gas phase oxidation was achieved by heating C-1 in 10% O₂/N₂ at 10 K min⁻¹ to 673 K for 12 h (denoted as C-5). C-5 was then heated in N₂ at 10 K min⁻¹ to 973 K for 1 h, producing the carbon carrier referred to as C-6. Platinum deposition occurred via the conventional wet impregnation method, whereby the carbon carriers were immersed in a solution of H₂PtCl₆ of the required concentration to result in a 1% w/w loading. The solution was then heated to 353 K until a slurry formed (~3 h) and then dried overnight at 383 K. The samples were then calcined in static air at 773 K for 4 h (10 K min⁻¹) and reduced in 10% H₂/N₂ at 573 K for 1 h (5 K min⁻¹), resulting in the active catalysts. All characterisation was performed on the active catalysts, i.e., after Pt deposition, calcination and reduction.

TPD spectra were obtained using a Micromeritics AutoChem II 2920 by heating the Pt/carbons (0.1 g) in a flow of He (20 mL min⁻¹) to 1173 K at a rate of 10 K min⁻¹. CO and CO₂ evolution was monitored using Hiden HPR20 mass spectrometer. XPS analysis was performed at the EPSRC National Facility for XPS with a Kratos Axis Supra utilising a monochromatic Al K α radiation source with an energy of 1486.7 eV. Electronic charge neutralization was achieved by using a low-energy electron flood

gun and magnetic immersion lens. The samples were affixed to the stage using copper tape and analysis took place under a vacuum of 1×10^{-9} Torr. All samples were calibrated using 284.5 eV of the C 1s peak. The percentage amount of oxygen and carbon was determined by integration of the peak areas and divided by the associated sensitivity factors (1.00 for C and 2.85 for O). Diffuse reflectance infrared Fourier transform spectra (DRIFTS) were obtained with a Shimadzu IRTracer-100. The catalyst samples were finely ground and diluted with KBr using a KBr/C mass ratio of 100. Pt loading was determined by inductively coupled plasma optical emission spectroscopy (Vista-PRO, Varian Inc.) after digestion in aqua regia at 523 K for 4 h. Pt morphology and average particle size were determined by transmission electron microscopy (TEM, Fei Tecnica G2 F20) by counting over 200 particles per sample. Samples were prepared by dispersing the catalyst powder in high purity ethanol, followed by sonication for 10 mins. A drop of this suspension was then evaporated on a holey carbon film supported by a 300 mesh copper TEM grid. Nitrogen adsorption/desorption isotherms were generated using an automated Micrometrics Tristar II 3000 Analyser and the surface area was determined using the BET method.

NAD(P)⁺ Regeneration.

The catalytic conversion of NAD(P)H to NAD(P)⁺ was carried out in a Radley Ready Duo reactor (100 mL) at 310 K, stirred at 300 rpm and using a flow of 30 mL min⁻¹ of N₂. In a typical experiment, 100 mL of 0.5 mM NADH (or NADPH) in a potassium phosphate buffer (0.1 M, pH 7 (or 10, 4) adjusted by a KOH or HCl solution) was loaded into the reactor, the N₂ gas was switched on and the system was heated to 310 K. When the temperature was reached and stable, 0.1 g of the catalyst was added, this point marking $t=0$. Aliquots of the reaction mixture were removed, filtered and then analysed. The consumption of NAD(P)H was monitored using a Jenway 6850 UV/Vis

spectrophotometer at 340 nm. NAD(P)⁺ concentration was determined by two methods, the first using an enzymatic cyclic assay (explained in detail below) and the second using UV/Vis. Both NAD(P)H and NAD(P)⁺ exhibit a λ_{max} of 260 nm due to the presence of the adenine moiety in both molecules but have different molar absorption coefficients. Hence, for any mixture of NAD(P)H and NAD(P)⁺, the concentration of NAD(P)⁺ can be determined if the concentration of NAD(P)H is known. Since the concentration of NAD(P)H can be determined by its λ_{max} at 340 nm (confirmed solely due to 1,4-NAD(P)H, see below), the contribution of NAD(P)H to the total absorbance at 260 nm of the mixture can be calculated and subtracted, and so whatever absorbance that remains at 260 nm is solely due to the NAD(P)⁺ in the system. Because the inactive isomers of NAD(P)H also contain chromophores with a λ_{max} of 260 nm, this method of NAD⁺ quantification was verified by comparison of the concentrations of NAD⁺ determined by the enzymatic cyclic assay, which showed excellent agreement.

As shown in [Figure S1](#), the cyclic assay utilises two enzymes (lactate dehydrogenase and diaphorase) and two substrates (lactate and MTT (3-(4,5-dimethylthiazol-2-yl)-2,5-diphenyltetrazolium bromide)) which are dependent on both NADH and NAD⁺. Tracking the formation of formazan (UV/Vis absorbance at 565 nm), the ultimate reduction product, allows for the quantification of both NADH and NAD⁺ in a given system.

To determine the concentration of 1,4-NADH in the system and to check that the absorbance at 340 nm was solely due to 1,4-NADH (i.e., no tautomerisation etc.), the reduction half of cyclic enzymatic assay was applied. Simply, MTT and diaphorase were added to the sample, and again tracking the formation of formazan will correspond to the concentration of 1,4-NADH in the system. Details about both

enzymatic assays are available in our previous work.²⁹ The conversion of NAD(P)H is defined by **Eq. (1)** and selectivity towards NAD(P)⁺ was calculated according to **Eq. (2)**. Repeated reactions with different samples from the same batch of catalyst delivered raw data that were reproducible to within $\pm 5\%$.

$$X_{\text{NAD(P)H}} (\%) = \frac{C_{\text{NAD(P)H,initial}} (\text{mM}) - C_{\text{NAD(P)H,left}} (\text{mM})}{C_{\text{NAD(P)H,initial}} (\text{mM})} \times 100 \quad (1)$$

$$\text{Yield}_{\text{NAD(P)}^+} (\%) = \frac{C_{\text{NAD(P)}^+} (\text{mM})}{C_{\text{NAD(P)H,initial}} (\text{mM})} \times 100 \quad (2)$$

Turnover frequency (TOF) was calculated using the initial rate based on NAD(P)H conversion and surface exposed Pt atoms. The moles of surface exposed Pt were estimated using Pt dispersion obtained from TEM particle size distributions, assuming spherical Pt nanoparticles. NADH in solution is known to undergo a first-order self-decay reaction,³⁰⁻³³ with, however, a neglectable rate constant (0.0011 min^{-1}) compared to our target catalytic oxidation.

Hydrogen Production.

The hydrogen production experiment was performed with a scaled-up concentration of NADH, ensuring that the volume of hydrogen formed was observable. 100 mL of 2 mM NADH solution in a 0.1 M, pH 7 phosphate buffer was added to a 100 mL round-bottom flask. This initial supply of NADH is equivalent to a theoretical yield of 4.8 mL of H₂. The round-bottom flask was connected via a PTFE line to an inverted measuring cylinder filled with water and suspended in a water bath (see [Figure S7](#)). The reaction mixture was purged with 30 mL min⁻¹ of N₂ for 20 mins and stirred at 600 rpm. After purging, Pt/C-6 (0.4 g) was added to commence the reaction at 293 K. After 100% conversion of NADH was achieved (determined by the absence of adsorption at 340 nm), the pH (remained at 7) and volume of gas produced were measured. The gas formed was analysed by a Shimadzu 2014C GC with a molecular sieve-13X column

(3.0 m × 3.2 mm) and a thermal conductivity detector (TCD). Data acquisition was performed using GC solution chromatography system.

The Expression and Purification of Alcohol Dehydrogenases.

The *E. coli* BL21(DE3) strains containing the protein expression plasmids of alcohol dehydrogenases were cultivated in the LB medium supplemented with 1.2% glycerol at 310 K. When A_{600} reached about 0.8, 500 μM isopropyl-beta-D-thiogalactopyranoside (IPTG, a final concentration) was added and the cultivation temperature was decreased to 291 K for ~16 h. After induction with 500 μM IPTG (final concentration), cells were harvested by centrifugation. The cell pellets were resuspended in 50 mM potassium phosphate buffer (pH 7.0), followed by sonification. After centrifugation, the supernatant was loaded onto the column packed with HisPur Ni-NTA Resin (Fisher Scientific, Pittsburgh, PA, USA) and eluted with 50 mM potassium phosphate buffer (pH 7.0) containing 300 mM NaCl and 250 mM imidazole. The purified proteins (10 μL were loaded into 12% sodium dodecyl sulphate–polyacrylamide gel electrophoresis (SDS-PAGE) to check the quality of purification.

Biocatalytic Alcohol Oxidations with *in situ* NAD⁺ Regeneration using the Pt/C-6 Catalyst.

The biocatalytic oxidative reactions catalysed by dehydrogenases with concurrent cofactor recycling were performed in 10 mL vials with a magnetic stir bar (10 mm × 3 mm) at room temperature (approximately 296 K), stirred at 600 rpm. 3 mL reaction mixture contained 50 mM potassium phosphate buffer (pH = 7.0), 2 mM alcohol substrate, 2% DMSO as cosolvent, 10 mg mL⁻¹ Pt/C-6 catalyst, 40 μM NADH, and 50 $\mu\text{g mL}^{-1}$ dehydrogenase. The headspace of the vials was filled with high purity N₂ gas. After 6 h of reaction, the products of the biocatalytic oxidative reaction were extracted

by using ethyl acetate and quantified using gas chromatography–mass spectrometry (GC-MS).

The GC-MS analysis was carried out using an Agilent 5975C GC/MSD instrument equipped with an Agilent DB-5MS column (30 m x 0.25 mm x 0.25 μm). The inlet temperature was held at 513 K with a 1.2 mL min^{-1} column flow rate and helium as the carrier gas. Reaction products were extracted with ethyl acetate containing 1 mM eicosane as an internal standard. 2 μL samples were manually injected onto the column. The oven temperature was held at 333 K for 1 min followed by a ramp to 473 K at a rate of 20 K min^{-1} . The integration value was recorded by GC/MSD data analysis. Control experiments using Pt/C-6, NADH and substrates (i.e., in the absence of enzymes) didn't generate any -OH oxidation products. Further control reactions using enzymes, NADH and substrates (i.e., in the absence of Pt/C-6) showed no products either.

Results and discussion

Pt/C Promoted Proton-Driven NAD⁺ Regeneration.

Initial experiments were undertaken with an unmodified Pt/C catalyst labelled as Pt/C-1. The catalyst was prepared by loading platinum onto an as-supplied activated carbon support, as described in the Supporting Information, and characterisation of the catalyst is described in the following section. [Figure 2a](#) shows the temporal consumption of NADH and the corresponding formation of NAD⁺ over this catalyst. Two different quantification methods for the NAD cofactors were applied to assess the selectivity of the catalyst. Since other enzymatically inactive isomers have a UV-Vis absorption in the same 340 nm region as NADH (such as the 1,6-NADH isomer (345 nm) and the (NAD)₂ dimers (~340 nm)), quantification by UV-Vis spectroscopy alone would be inconclusive for NADH conversion and so enzymatic assays were applied

(Figure S1).²⁹ It was found that after 45 mins of reaction, 100% conversion of NADH was achieved with a yield of 91% of NAD⁺. The exponential shape of NADH consumption throughout time indicates a first-order reaction with respect to NADH consumption (Figure S2). The derived rate constant was 7.4 h⁻¹. This equates to an initial turnover frequency (TOF, i.e., molecules of NADH reacted per surface platinum active site per time) of 105 h⁻¹. Monitoring the total concentration of NADH and NAD⁺ in the system reveals that during the initial stage of reaction, 9% of total NAD in the system is lost. After this period, the amount of total NAD remains constant throughout the course of the reaction, meaning that 100% of the NADH is being converted to NAD⁺.

This behaviour resulted in the proposed hypothesis that the initial loss of cofactors in the system was due to the adsorption of NADH or NAD⁺ onto the catalyst surface as opposed to the unselective conversion of NADH. The absence of any byproduct peaks in the UV-Vis profiles (Figure 2b) supports this hypothesis, but to verify this, adsorption experiments were conducted whereby both NADH and NAD⁺ were separately exposed to the untreated carbon carrier (C-1, before Pt deposition) to remove the catalytic influence of Pt and to see which cofactor, if any, would undergo adsorption. Figure S3 shows that the concentration of NADH in solution decreases at the same rate as the known NADH decomposition/decay^{30,32,34} (in the absence of C-1) under the experimental conditions, meaning no adsorption took place. But interestingly, there was a clear decrease in NAD⁺ concentration, revealing that the loss of selectivity during the course of the reaction was caused by the adsorption/immobilisation of NAD⁺ onto the carbon support. To further verify this, the same adsorption experiment was repeated with Pt/C-1 and NAD⁺ (Figure S3), which resulted in the same amount of NAD⁺ being adsorbed. In other words, all of the NADH in the regeneration reaction is

selectively converted to the target NAD^+ , part of which, however, remains on the catalyst via adsorption.

The majority of NAD^+ -dependent enzymes have a working pH range of 7-10, and so the influence of proton concentration on the regeneration of NAD^+ was examined. Due to the instability of NADH, particularly in acidic environments, blank reactions were initially performed and are shown in [Figure S4](#). In agreement with the literature,³⁵ the decay of NADH was heavily proton dependent with first-order rate constants of NADH decay of 1.59, 0.66 and 0.012 h^{-1} at pH 4, 7 and 10, respectively. Temporal NADH conversion profiles ([Figure 2c](#)) reveal reduced activity with decreasing proton concentration with corresponding rate constants (after removing the decay effect) of 14.6, 7.44 and 1.92 h^{-1} . This provides good evidence of the proton-driven reaction proposed in [Figure 1b](#) (H_2 production will be discussed in the following section). This first attempt of creating a NAD(H)-dependent hydrogenase biomimetic that can also immobilise NAD^+ and operate under the reaction conditions preferred by NAD^+ -dependent enzymes via heterogeneous supported Pt catalyst has thus proven feasible.

Catalyst Optimisation.

TEM images of the Pt/C-1 catalyst ([Figure 3a](#)) show that it contains highly dispersed Pt nanoparticles with a mean particle size of 2.6 nm ([Figure 3b](#)). It is well known that the electronic character of the Pt active sites on carbon supports can be selectively tuned by modifying the surface chemistry of the carbon, which is particularly useful in oxidation reactions.^{36,37} We considered that if the platinum is mimicking the function of NAD(H)-linked hydrogenases in the natural system by promoting the reduction of protons to hydrogen, this may be enhanced with higher electron density on the platinum.³⁸ In fact, hydrogenases contain iron-sulfur clusters that act as an electron

reservoir to promote proton reduction, therefore it would be reasonable to assume that creating an electron reservoir in the Pt active sites would enhance the rate of reaction in our system.³⁹ We therefore prepared a series of platinum catalysts of the same loading on modified carbon supports with the aim of enhancing the activity for NAD⁺ regeneration. In brief, liquid phase oxidation treatments of the carbon employed either HNO₃ (5 M: Pt/C-2, 10 M: Pt/C-3) or H₂O₂ (Pt/C-4), while gas phase oxidation used O₂ (Pt/C-5) followed by heating in nitrogen at 973 K prior to platinum deposition (Pt/C-6).

Figure 4a,b shows the CO₂ and CO TPD spectra of the Pt/C catalysts with the activated carbon before (Pt/C-1) and after various liquid and gas-phase oxidative treatments (Pt/C-2-6). Liquid-phase treatments of the carbon with 5 (Pt/C-2) and 10 M HNO₃ (Pt/C-3) cause an increase in CO₂ evolution at lower temperatures (473-873 K at a maximum of ~573 K) characteristic of carboxylic acid groups being formed. H₂O₂ treatment (Pt/C-4) resulted in CO₂ evolution at both low and high temperatures, with maximums of about 573 and 1010 K. The CO₂ profiles for the gas phase oxidised samples are dominated by high temperature peaks characteristic of lactone or anhydride groups.⁴⁰ The CO desorption profiles are quite similar for all of the carbons. Deconvolution of the O 1s peak (Figure 4c) at 531.4, 532.3, 533.2 and 534.3 eV indicates the type of functionalities that contribute to these peaks, whereby a binding energy of 531.4 eV corresponds to quinone type carbonyls, 532.3 eV for carbonyl oxygen atoms in anhydrides and lactones and oxygen atoms in phenolic and ether groups, 533.2 eV for ether oxygen atoms in lactones and anhydrides and 534.3 eV which corresponds to oxygen groups in carboxylic acids.⁴¹ The most noticeable difference in the O 1s profiles are in the growth of a higher binding energy component at 534.4 eV characteristic of carboxylic acid groups, but this component is

conspicuously absent from the gas-phase oxidised carbons. The O 1s profiles for Pt/C-5 and Pt/C-6 closely resemble those of Pt/C-1. [Figure 4d](#) shows the DRIFTS spectra recorded before and after different oxidative treatments. As with the XPS O1s spectra, the most obvious differences are seen for the liquid-phase oxidised samples (Pt/C-2-4), which show enhanced bands above 1600 cm^{-1} characteristic of carboxylic acid groups. Gas phase oxidation in O_2 (Pt/C-5) is known to incorporate hydroxyl and carbonyl surface groups (e.g., phenolic, lactonic and anhydride functionalities).⁴⁰ The subsequent thermal treatment at 973 K in N_2 of Pt/C-6 will result in the decomposition of the surface groups that are unstable below this temperature, which is evidenced by the lack of any significant peaks in the CO_2 TPD spectra of Pt/C-6 ([Figure 4a](#)).

TEM images showed that all of the platinum loaded catalysts contained highly dispersed platinum nanoparticles ([Figure 3](#) and [Figure S5](#)) although some differences in mean particle size and size distribution were noted ([Table 1](#)). Clear differences in the Pt 4f XPS binding energies with support pre-treatment were seen ([Figure 5a](#)). Liquid phase oxidative treatments (Pt/C-2,3,4) increased the binding energy relative to Pt/C-1, whereas the gas phase oxidation of the support decreased the binding energy below that of Pt/C-1. Binding energies of supported platinum and other metal clusters are influenced both by cluster size effects (decreasing cluster size increases binding energies) and support interactions.⁴² O 1s XPS spectra, DRIFTS and CO/CO_2 TPD measurements ([Figure 4](#)) show that the liquid phase oxidative treatments of the carbon supports produces carboxylate surface groups, and it may be argued that the interaction of these electron withdrawing groups with the Pt clusters lowers the electron density on the platinum, increasing the Pt 4f binding energy. On the other hand, the two gas-phase treated samples, likely due to the overall electron-donating

effects of the groups present and the increased Pt size (in the case of Pt/C-6, [Table 1](#)), exhibited a decrease in the Pt 4f binding energy.

The higher electron density on the Pt clusters in Pt/C-5 and Pt/C-6 does result in a higher activity for NAD⁺ regeneration than Pt/C-1. This is seen in the conversion versus time plots in [Figure 5b](#). On the other hand, the catalysts with lower Pt electron density (Pt/C-2,3,4) are less active than Pt/C-1. These differences become more apparent when initial turnover frequencies (TOF = NADH molecules converted per surface exposed Pt atom per unit time) are plotted against the Pt 4f_{7/2} binding energy in [Figure 5c](#). There is a clear correlation: higher electron density on the Pt results in higher TOF, and the most active catalyst, Pt/C-6, has an initial TOF ~6 times higher than Pt/C-1 and ~8 times higher than the reported Au/Nb₂O₅¹³ (73.4 h⁻¹ using O₂ but inactive using protons).

To further confirm the role of electron-rich Pt in promoting the reduction of protons to hydrogen we measured the hydrogen produced in a NAD⁺ regeneration reaction using Pt/C-6. Under the reaction conditions employed 4.6 mL of H₂ was produced from a theoretical yield of 4.8 mL (see [Figure S6](#)). This provides clear evidence of stoichiometric H₂ production (within the accuracy range expected for the experiment) in the proton-driven NADH oxidation (i.e., NADH + H⁺ = NAD⁺ + H₂). It should be noted here that this is for the first time the above chemical reaction is catalysed by a heterogeneous supported metal catalyst. The other important oxidized nicotinamide cofactor is its phosphorylated form, i.e., NADP⁺. The Pt/C-6 catalyst was subsequently examined in the NADPH dehydrogenation for NADP⁺ regeneration ([Figure S7](#)), where a very similar catalytic response (to that of NAD⁺) was obtained, with a TOF of 560 h⁻¹. The optimised Pt/C-6 catalyst was then employed in all of the subsequent experiments described below.

Biocatalytic Alcohol Oxidations with *in situ* NAD⁺ Regeneration using the Pt/C-6 Catalyst.

Cooperative catalysis requires chemo-enzymatic systems to be mutually compatible, which is often difficult to obtain.⁴³ When applied independently, the inorganic and enzymatic catalysts typically operate under different reaction conditions (temperature, pH, solvent etc.) and are also known to cause mutual deactivation.⁴⁴⁻⁴⁷ Although we have proved the regeneration capability of supported Pt catalysts, the inorganic catalyst must successfully work in conjunction with the enzyme to demonstrate the feasibility of this cooperative system for sustainable chemical production. In order to illustrate the NAD⁺ regeneration ability of Pt/C-6 to support biocatalytic oxidations, the oxidation of alcohols catalysed by different alcohol dehydrogenases was studied as a model system. As shown in [Table 2](#), four different alcohols were selected as model substrates and included primary and secondary aliphatic alcohols, an aliphatic diol and an aromatic secondary alcohol, showing the versatility of the cooperative system.

The oxidation of the four alcohol substrates were catalysed by four alcohol dehydrogenases from different microorganisms (TesADH: alcohol dehydrogenase from *Thermoanaerobacter ethanolicus*; ADH-hT: alcohol dehydrogenase from *Geobacillus stearothermophilus*; AA-ADH: (S)-Specific 1-phenylethanol dehydrogenase of the denitrifying *Bacterium* Strain EbN1; HL-ADH: alcohol dehydrogenase E chain of horse, [Figure S8](#)) and was integrated with the NAD⁺ regeneration system based on the Pt/C-6 catalyst, respectively. After 6 h of reaction starting with NADH (which would be inactive in the absence of regeneration), all four alcohol substrates were converted to corresponding ketone and lactone products. On the contrary, for the reaction system without Pt/C-6 catalyst, the products were not

detectable. This result clearly demonstrated that the Pt/C-6 catalyst possessed the compatibility with biocatalytic systems, which could be utilised to realise NAD⁺ regeneration and support biocatalytic alcohol oxidation. The conversion of different substrates showed a significant difference. The conversion of (S)-(+)-2-octanol achieved 58%, meanwhile the conversion of 1-heptanol was only 6.5%. This difference is caused by the difference in the specific activity of enzymes to different substrates.

In general, the application of heterogeneous catalysts to perform effective cofactor regeneration and further drive the enzymatic conversion, even multi-enzyme cascade conversion, provides a promising strategy to realise the industrial application of biocatalysis. In addition to reducing the cost of using cofactor, the heterogeneous catalyst offers significant downstream separation advantages and can be recycled in comparison with homogeneous catalysts. The Pt/C-6 catalyst developed in this study further has the advantage of being robust and convenient to use. Without the input of external photo or electrical energy and the construction of an additional reaction system (e.g., reactor compartmentation), the Pt/C-6 catalyst simply promotes oxidation of NADH using protons and is compatible with the enzymatic oxidations which in turn produce the required protons.

Conclusions

In summary, a heterogeneous catalyst formulation was designed to promote proton-driven oxidation of NAD(P)H to NAD(P)⁺ with concurrent hydrogen formation. The resulting Pt/C-6 catalyst with the highest degree of electron donation from carbon generated the highest TOF (581 h⁻¹ for NADH consumption; 560 h⁻¹ for NADPH consumption): a result of electron-rich Pt promoted electron transfer to protons. The Pt/C-6 exhibited good compatibility with biocatalytic systems and support the oxidation

of different alcohols catalysed by alcohol dehydrogenases from different microorganisms. This work provides a promising strategy for chemical synthesis via NAD(P)⁺-dependent pathways, utilising a cooperative inorganic-enzymatic catalytic system.

ASSOCIATED CONTENT

Supporting Information. This Supporting Information is available free of charge via the Internet at <http://pubs.acs.org>. Amino acid sequences of alcohol dehydrogenases used in this study, first order kinetics of NADH consumption and decay of NADH under reaction conditions, the adsorption of NAD⁺ on C-1 and Pt/C-1, decay of NADH at different pH, TEM images at different resolutions and the corresponding Pt particle size histograms for the Pt/C-2-5 catalysts, experiment of hydrogen production, SDS-PAGE analysis of purified enzymes used for biocatalytic alcohol oxidations.

AUTHOR INFORMATION

Corresponding Author

*Shelley D. Minteer: minteer@chem.utah.edu; *Xiaodong Wang: xiaodong.wang@lancaster.ac.uk

Author contributions

J. W. H. B., H. C., J. L. and Y. L. performed the experiments. All authors analyzed the data and co-wrote the article. All authors have given approval to the final version of the article. †J. W. H. B. and †H. C. contributed equally to this work.

Acknowledgments

This work was supported by the EPSRC New Horizons scheme (EP/V048635/1), Royal Society (ICA\R1\180317) and National Science Foundation Center for Synthetic Organic Electrochemistry (2002158). We are also grateful for support from the UK Catalysis Hub funded by EPSRC grant reference EP/R026645/1.

Notes

The authors declare no competing interests.

References

- (1) Chen, H.; Dong, F.; Minter, S. D. The Progress and Outlook of Bioelectrocatalysis for the Production of Chemicals, Fuels and Materials. *Nature Catal.* **2020**, 3 (3), 225-244.
- (2) Prier, C. K.; Kosjek, B. Recent Preparative Applications of Redox Enzymes. *Curr. Opin. Chem. Biol.* **2019**, 49, 105-112.
- (3) Bornscheuer, U. T.; Huisman, G.; Kazlauskas, R.; Lutz, S.; Moore, J.; Robins, K. Engineering the Third Wave of Biocatalysis. *Nature* **2012**, 485 (7397), 185-194.
- (4) Koeller, K. M.; Wong, C.-H. Enzymes for Chemical Synthesis. *Nature* **2001**, 409 (6817), 232-240.
- (5) Litman, Z. C.; Wang, Y.; Zhao, H.; Hartwig, J. F. Cooperative Asymmetric Reactions Combining Photocatalysis and Enzymatic Catalysis. *Nature* **2018**, 560 (7718), 355-359.
- (6) Tseliou, V.; Knaus, T.; Masman, M. F.; Corrado, M. L.; Mutti, F. G. Generation of Amine Dehydrogenases with Increased Catalytic Performance and Substrate Scope from E-Deaminating L-Lysine Dehydrogenase. *Nature Commun.* **2019**, 10 (1), 1-11.
- (7) Li, X.; Cao, Y.; Luo, K.; Sun, Y.; Xiong, J.; Wang, L.; Liu, Z.; Li, J.; Ma, J.; Ge, J. Highly Active Enzyme–Metal Nanohybrids Synthesized in Protein–Polymer Conjugates. *Nature Catal.* **2019**, 2 (8), 718-725.
- (8) Wang, Z. J.; Clary, K. N.; Bergman, R. G.; Raymond, K. N.; Toste, F. D. A Supramolecular Approach to Combining Enzymatic and Transition Metal Catalysis. *Nature Chem.* **2013**, 5 (2), 100-103.
- (9) Liu, J.; Wu, S.; Li, Z. Recent Advances in Enzymatic Oxidation of Alcohols. *Curr. Opin. Chem. Biol.* **2018**, 43, 77-86.

- (10) Hollmann, F.; Arends, I. W. C. E.; Buehler, K.; Schallmeyer, A.; Bühler, B. Enzyme-Mediated Oxidations for the Chemist. *Green Chem.* **2011**, *13* (2), 226-265.
- (11) Faber, K. Biocatalytic Applications. *Biotransformations in Organic Chemistry: A Textbook*, Springer International Publishing, 2018; p 134.
- (12) Mordhorst, S.; Andexer, J. N. Round, Round We Go—Strategies for Enzymatic Cofactor Regeneration. *Nat. Prod. Rep.* **2020**, *37* (10), 1316-1333.
- (13) Nishigaki, J.-i.; Ishida, T.; Honma, T.; Haruta, M. Oxidation of B-Nicotinamide Adenine Dinucleotide (NADH) by Au Cluster and Nanoparticle Catalysts Aiming for Coenzyme Regeneration in Enzymatic Glucose Oxidation. *ACS Sust. Chem. & Eng.* **2020**, *8* (28), 10413-10422.
- (14) Wu, H.; Tian, C.; Song, X.; Liu, C.; Yang, D.; Jiang, Z. Methods for the Regeneration of Nicotinamide Coenzymes. *Green Chem.* **2013**, *15* (7), 1773-1789.
- (15) Kochius, S.; Magnusson, A. O.; Hollmann, F.; Schrader, J.; Holtmann, D. Immobilized Redox Mediators for Electrochemical NAD(P)⁺ Regeneration. *Appl. Microbiol. Biotechnol.* **2012**, *93* (6), 2251-2264.
- (16) Liu, W.; Wang, P. Cofactor Regeneration for Sustainable Enzymatic Biosynthesis. *Biotechnol. Adv.* **2007**, *25* (4), 369-384.
- (17) Song, H.; Ma, C.; Wang, L.; Zhu, Z. Platinum Nanoparticle-Deposited Multi-Walled Carbon Nanotubes as a NADH Oxidase Mimic: Characterization and Applications. *Nanoscale* **2020**, *12* (37), 19284-19292.
- (18) Zhuang, M. Y.; Jiang, X. P.; Ling, X. M.; Xu, M. Q.; Zhu, Y. H.; Zhang, Y. W. Immobilization of Glycerol Dehydrogenase and NADH Oxidase for Enzymatic Synthesis of 1, 3-Dihydroxyacetone with in Situ Cofactor Regeneration. *J. Chem. Technol. Biotechnol.* **2018**, *93* (8), 2351-2358.
- (19) Zhang, J.; Cui, Z.; Chang, H.; Fan, X.; Zhao, Q.; Wei, W. Conversion of Glycerol to 1, 3-Dihydroxyacetone by Glycerol Dehydrogenase Co-Expressed with an NADH Oxidase for Cofactor Regeneration. *Biotechnol. Lett.* **2016**, *38* (9), 1559-1564.
- (20) Geueke, B.; Riebel, B.; Hummel, W. NADH Oxidase from *Lactobacillus Brevis*: A New Catalyst for the Regeneration of NAD. *Enzyme Microb. Technol.* **2003**, *32* (2), 205-211.
- (21) Staffell, I.; Scamman, D.; Abad, A. V.; Balcombe, P.; Dodds, P. E.; Ekins, P.; Shah, N.; Ward, K. R. The Role of Hydrogen and Fuel Cells in the Global Energy System. *Energy Environ. Sci.* **2019**, *12* (2), 463-491.

- (22) Kim, S.; Lee, G. Y.; Baeg, J.-O.; Kim, Y.; Kim, S.-J.; Kim, J. Visible-Light-Driven Photoproduction of Hydrogen Using Rhodium Catalysts and Platinum Nanoparticles with Formate. *J Phys. Chem. C* **2014**, *118* (45), 25844-25852.
- (23) Reeve, H. A.; Lauterbach, L.; Ash, P. A.; Lenz, O.; Vincent, K. A. A Modular System for Regeneration of NAD Cofactors Using Graphite Particles Modified with Hydrogenase and Diaphorase Moieties. *Chem. Commun.* **2012**, *48* (10), 1589-1591.
- (24) Betanzos-Lara, S.; Liu, Z.; Habtemariam, A.; Pizarro, A. M.; Qamar, B.; Sadler, P. J. Organometallic Ruthenium and Iridium Transfer-Hydrogenation Catalysts Using Coenzyme NADH as a Cofactor. *Angew. Chem.* **2012**, *124* (16), 3963-3966.
- (25) Hambourger, M.; Brune, A.; Gust, D.; Moore, A. L.; Moore, T. A. Enzyme-Assisted Reforming of Glucose to Hydrogen in a Photoelectrochemical Cell. *Photochem. Photobiol.* **2005**, *81* (4), 1015-1020.
- (26) Maenaka, Y.; Suenobu, T.; Fukuzumi, S. Efficient Catalytic Interconversion between NADH and NAD⁺ Accompanied by Generation and Consumption of Hydrogen with a Water-Soluble Iridium Complex at Ambient Pressure and Temperature. *J. Am. Chem. Soc.* **2012**, *134* (1), 367-374.
- (27) Poizat, M.; Arends, I. W.; Hollmann, F. On the Nature of Mutual Inactivation between [Cp* Rh (Bpy)(H₂O)]²⁺ and Enzymes—Analysis and Potential Remedies. *J. Mol. Catal. B: Enzym.* **2010**, *63* (3-4), 149-156.
- (28) Rothenberg, G. *Catalysis: Concepts and Green Applications*; John Wiley & Sons, 2017.
- (29) Saba, T.; Burnett, J. W. H.; Li, J.; Kechagiopoulos, P.; Wang, X. A Facile Analytical Method for Reliable Selectivity Examination in Cofactor NADH Regeneration. *Chem. Commun.* **2020**, *56* (8), 1231-1234.
- (30) Saba, T.; Li, J. W.; Burnett, J. W. H.; Howe, R. F.; Kechagiopoulos, P. N.; Wang, X. NADH Regeneration: A Case Study of Pt-Catalyzed NAD⁺ Reduction with H₂. *ACS Catal.* **2021**, *11* (1), 283-289.
- (31) Alivisatos, S. G.; Ungar, F.; Abraham, G. J. Spontaneous Reactions of 1, 3-Substituted 1, 4-Dihydropyridines with Acids in Water at Neutrality. I. Kinetic Analysis and Mechanism of the Reactions of Dihyronicotinamide-Adenine Dinucleotide with Orthophosphates. *Biochem.* **1965**, *4* (12), 2616-2630.

- (32) Li, H.; Worley, K. E.; Calabrese Barton, S. Quantitative Analysis of Bioactive NAD⁺ Regenerated by NADH Electro-Oxidation. *ACS Catal.* **2012**, *2* (12), 2572-2576.
- (33) Jones, W.; Burnett, J. W. H.; Shi, J.; Howe, R. F.; Wang, X. Improving Photocatalytic Energy Conversion via NAD(P)H. *Joule.* **2020**, *4* (10), 2055-2059.
- (34) Anderson Jr, A. G.; Berkelhammer, G. A Study of the Primary Acid Reaction on Model Compounds of Reduced Diphosphopyridine Nucleotide. *J. Am. Chem. Soc.* **1958**, *80* (4), 992-999.
- (35) Rover Jr, L.; Fernandes, J. C.; de Oliveira Neto, G.; Kubota, L. T.; Katekawa, E.; Serrano, S. H. Study of NADH Stability Using Ultraviolet–Visible Spectrophotometric Analysis and Factorial Design. *Anal. Biochem.* **1998**, *260* (1), 50-55.
- (36) Yang, Z.; Pedireddy, S.; Lee, H. K.; Liu, Y.; Tjiu, W. W.; Phang, I. Y.; Ling, X. Y. Manipulating the D-Band Electronic Structure of Platinum-Functionalized Nanoporous Gold Bowls: Synergistic Intermetallic Interactions Enhance Catalysis. *Chem. Mater.* **2016**, *28* (14), 5080-5086.
- (37) Şen, F.; Gökağaç, G. Different Sized Platinum Nanoparticles Supported on Carbon: An XPS Study on These Methanol Oxidation Catalysts. *J Phys. Chem. C* **2007**, *111* (15), 5715-5720.
- (38) Ghosh, S.; Hollingsworth, N.; Warren, M.; Hrovat, D. A.; Richmond, M. G.; Hogarth, G. Hydrogenase Biomimics containing Redox-active Ligands: Fe₂(CO)₄(μ-edt)(κ²-bpcd) with Electron-acceptor 4,5-bis(diphenylphosphino)-4-cyclopenten-1,3-dione (bpcd) as A Potential [Fe₄-S₄]_H Surrogate. *Dalton Trans.* **2019**, *48* (18), 6051-6060.
- (39) Becker, R.; Amirjalayer, S.; Li, P.; Woutersen, S.; Reek, J. N. An Iron-Iron Hydrogenase Mimic with Appended Electron Reservoir for Efficient Proton Reduction in Aqueous Media. *Science Adv.* **2016**, *2* (1), e1501014.
- (40) Zhou, J.-H.; Sui, Z.-J.; Zhu, J.; Li, P.; Chen, D.; Dai, Y.-C.; Yuan, W.-K. Characterization of Surface Oxygen Complexes on Carbon Nanofibers by TPD, XPS and FT-IR. *Carbon* **2007**, *45* (4), 785-796.
- (41) Lennon, D.; Lundie, D.; Jackson, S.; Kelly, G.; Parker, S. Characterization of Activated Carbon Using X-Ray Photoelectron Spectroscopy and Inelastic Neutron Scattering Spectroscopy. *Langmuir* **2002**, *18* (12), 4667-4673.
- (42) Isaifan, R. J.; Ntais, S.; Baranova, E. A. Particle Size Effect on Catalytic Activity of Carbon-Supported Pt Nanoparticles for Complete Ethylene Oxidation. *Appl. Catal. A: Gen.* **2013**, *464*, 87-94.

- (43) Rudroff, F.; Mihovilovic, M. D.; Gröger, H.; Snajdrova, R.; Iding, H.; Bornscheuer, U. T. Opportunities and Challenges for Combining Chemo-and Biocatalysis. *Nature Catal.* **2018**, *1* (1), 12-22.
- (44) Köhler, V.; Turner, N. J. Artificial Concurrent Catalytic Processes Involving Enzymes. *Chem. Commun.* **2015**, *51* (3), 450-464.
- (45) Denard, C. A.; Huang, H.; Bartlett, M. J.; Lu, L.; Tan, Y.; Zhao, H.; Hartwig, J. F. Cooperative Tandem Catalysis by an Organometallic Complex and a Metalloenzyme. *Angew. Chem. Int. Ed.* **2014**, *53* (2), 465-469.
- (46) Köhler, V.; Wilson, Y.; Dürrenberger, M.; Ghislieri, D.; Churakova, E.; Quinto, T.; Knörr, L.; Häussinger, D.; Hollmann, F.; Turner, N. Synthetic Cascades Are Enabled by Combining Biocatalysts with Artificial Metalloenzymes. *Nature Chem.* **2013**, *5* (2), 93-99.
- (47) Haak, R. M.; Berthiol, F.; Jerphagnon, T.; Gayet, A. J.; Tarabiono, C.; Postema, C. P.; Ritleng, V.; Pfeffer, M.; Janssen, D. B.; Minnaard, A. J. Dynamic Kinetic Resolution of Racemic B-Haloalcohols: Direct Access to Enantioenriched Epoxides. *J. Am. Chem. Soc.* **2008**, *130* (41), 13508-13509.

Figures

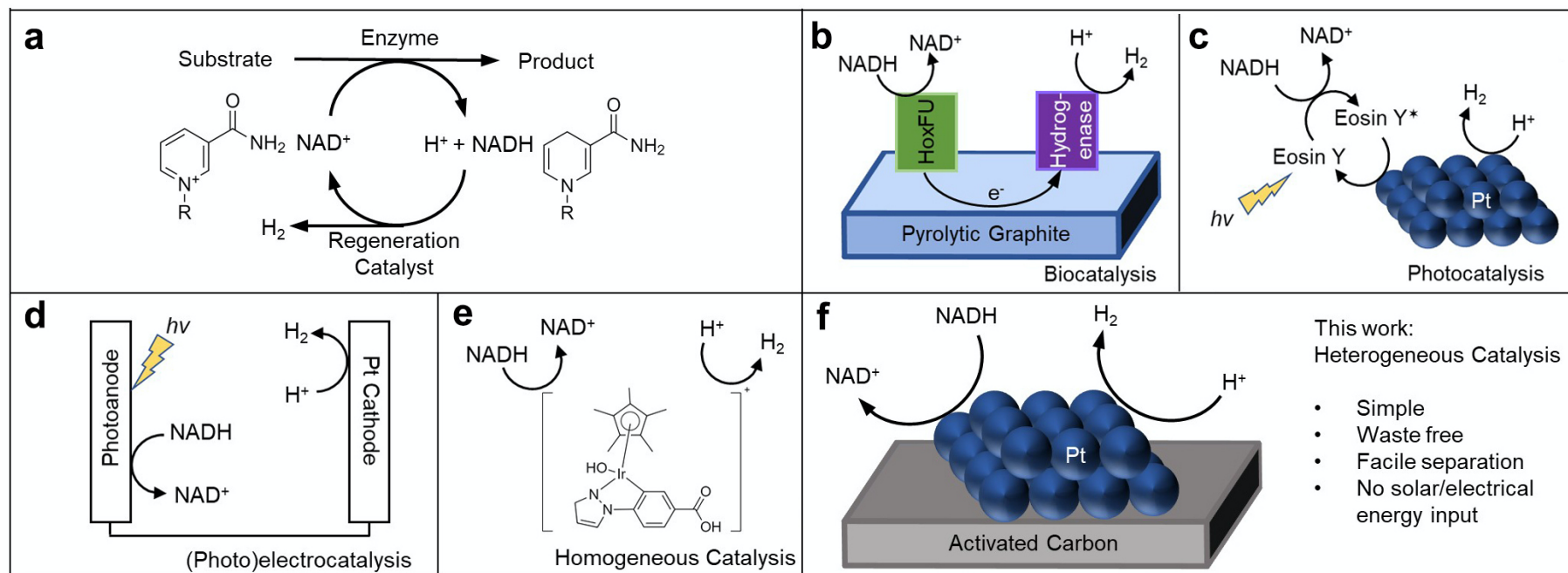


Figure 1: **a**, Schematic showing a general enzymatic oxidation with the concurrent consumption of NAD^+ , coupled to the regeneration of NAD^+ via a proton-driven regeneration catalyst. **b-e**, Existing methods of proton-driven NAD^+ regeneration. **b** shows a biocatalytic example that utilises two enzymes supported on pyrolytic graphite, whereby the enzyme HoxFU catalyses the conversion of NADH to NAD^+ . The electrons produced from this reaction are transferred via the support to the hydrogenase enzyme that converts protons to hydrogen. **c** uses the photosensitiser Eosin Y to convert NADH to NAD^+ and the electron formed are utilised by platinum nanoparticles to convert protons to hydrogen. **d** uses a photoanode to convert NADH to NAD^+ and a platinum cathode is used to transfer the electrons to protons to form hydrogen. **e** uses an iridium organometallic complex to convert NADH to NAD^+ and transfer the electrons to protons, forming hydrogen. **f**, Proton-driven NAD^+ regeneration using supported Pt (this work).

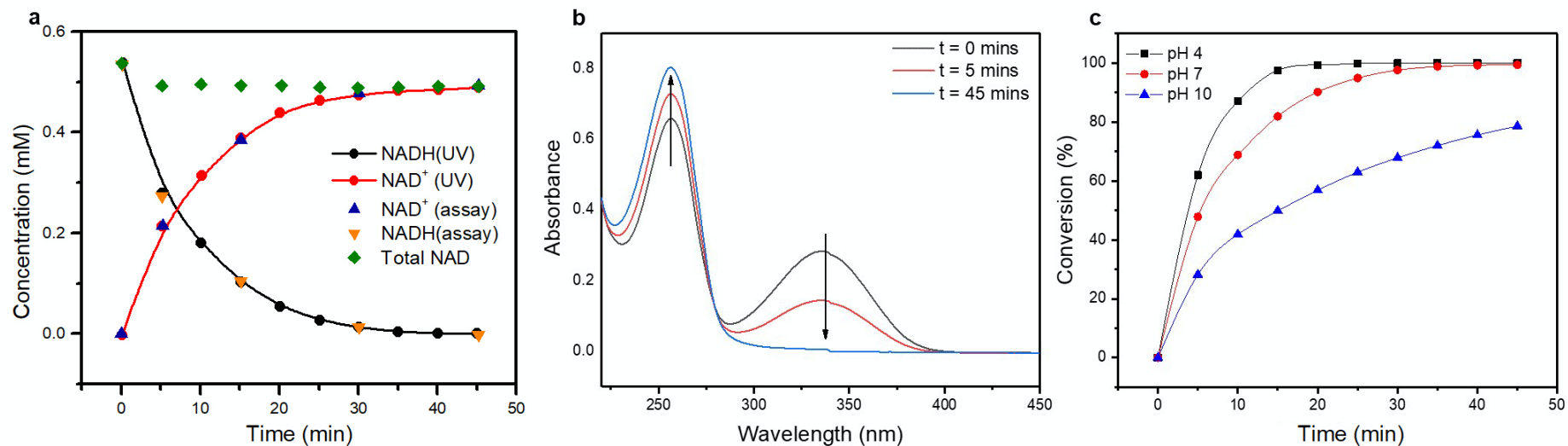


Figure 2: **a**, Temporal consumption of NADH and concurrent formation of NAD⁺ over Pt/C-1. Determination of the concentration of NADH and NAD⁺ by UV-Vis (black line with symbols) and enzymatic assays (red symbols). Total concentration of NADH and NAD⁺ determined by enzymatic assays (open diamonds). **b**, Corresponding UV-Vis spectra at 0, 5 and 45 mins of reaction. **c**, Temporal conversion of NADH at various pH. Reaction conditions: 0.5 mM of NADH in 100 mL of phosphate buffer (0.1 M, pH 7 for **a,b**), 0.1 g of Pt/C-1, 30 mL min⁻¹ of N₂ and at 310 K.

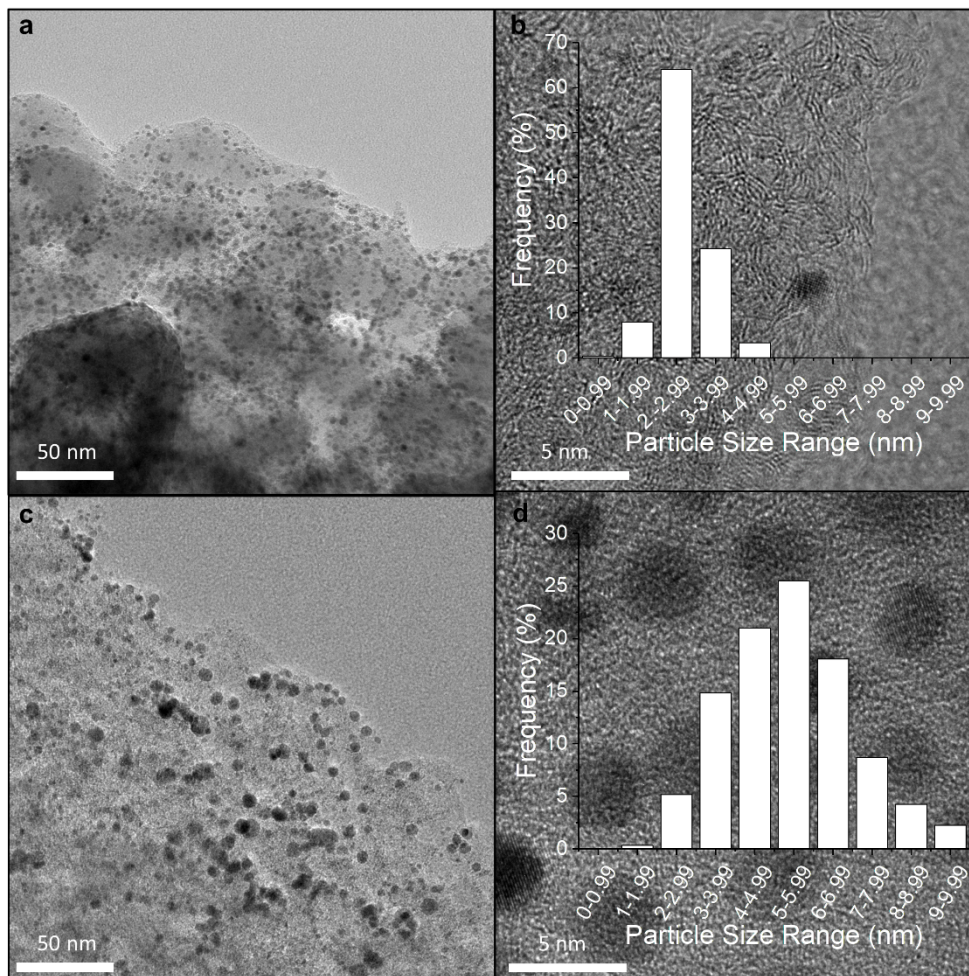


Figure 3: Representative TEM images at different resolutions with the corresponding particle size histograms for Pt/C-1 (a, b) and Pt/C-6 (c, d), respectively.

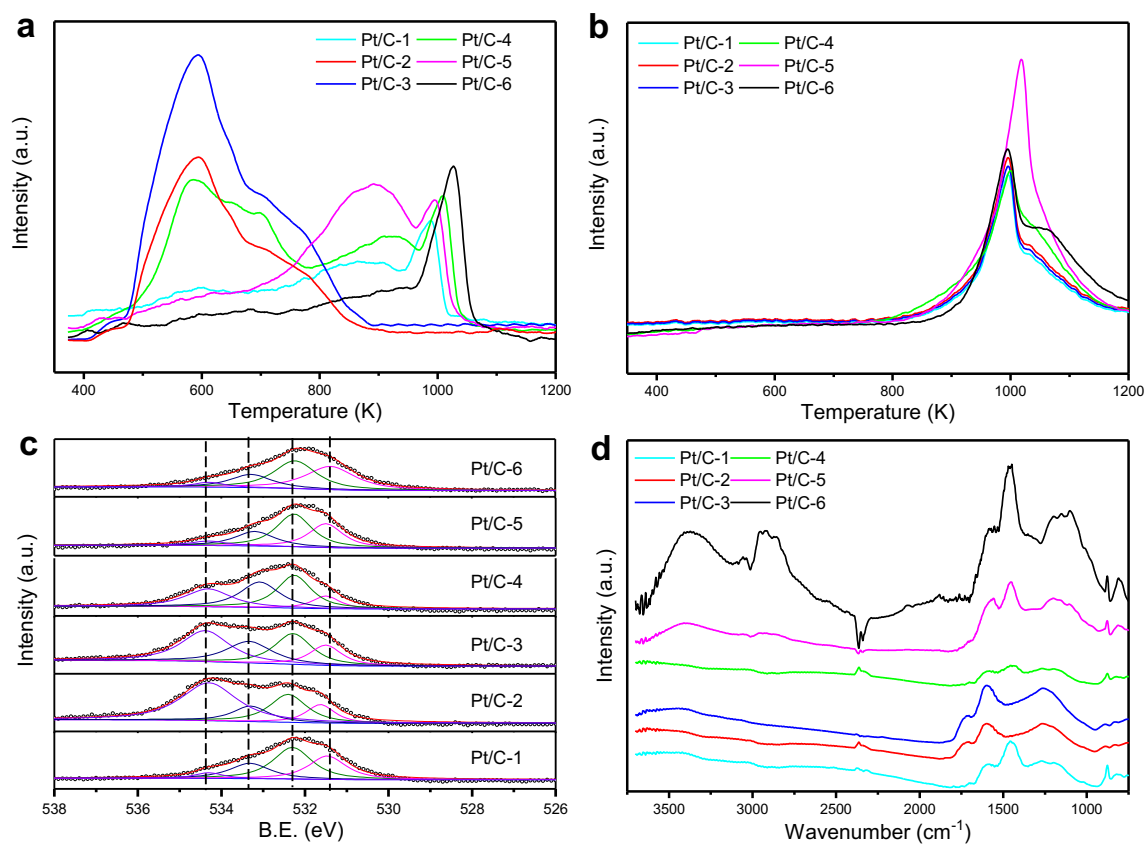


Figure 4: Characterisation of the Pt/C catalysts showing **a**, CO₂ TPD profiles, **b**, CO TPD profiles, **c**, O1s XPS spectra with deconvolution at 531.4, 532.3, 533.2 and 534.3 eV (circle: raw data) and **d**, DRIFTS spectra.

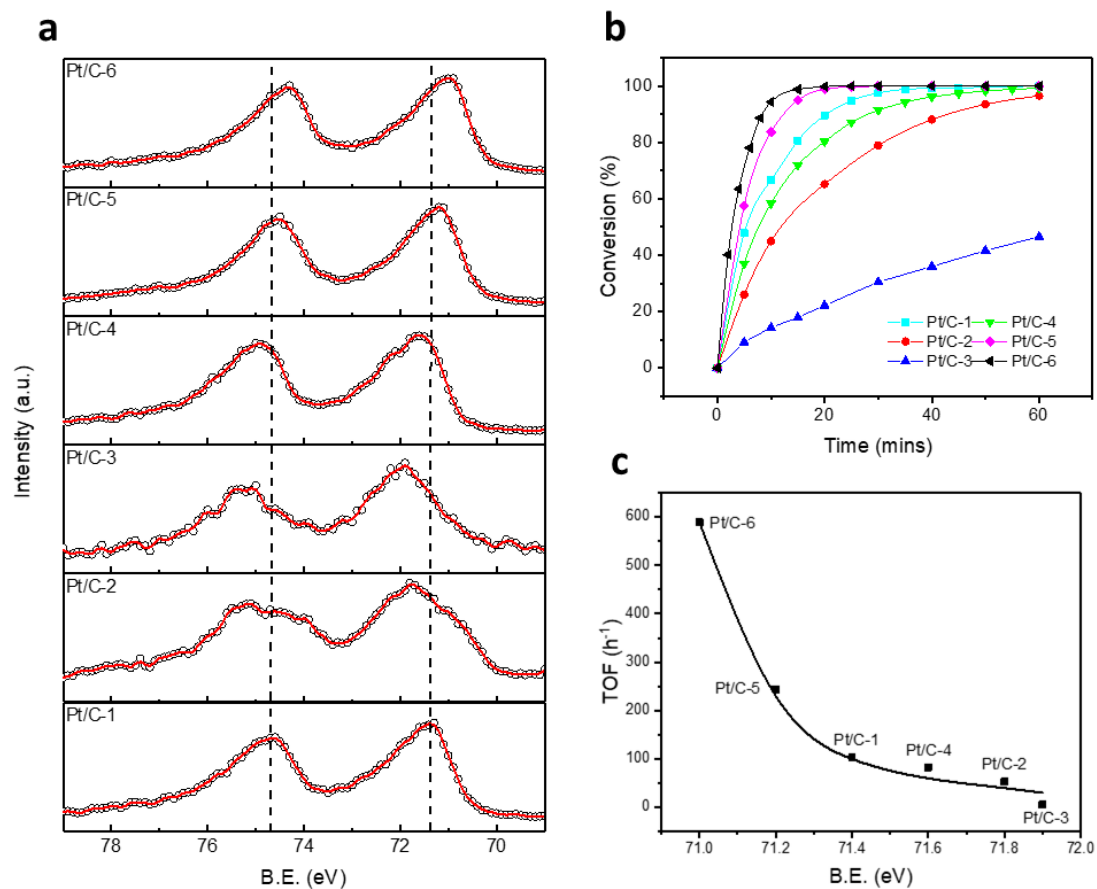


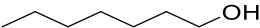

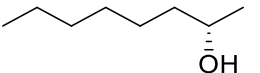
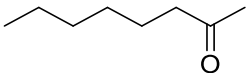
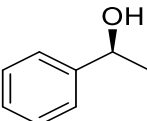
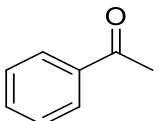

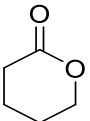
Figure 5: **a**, Pt 4f spectra of the Pt/C catalysts. Circles: experimental data; red lines: fitting of raw data; dashed lines: original Pt 4f peak position of the doublet observed in Pt/C-1. **b**, Comparison of the activities of Pt/C catalysts. **c**, Relationship between the TOF and Pt 4f B.E. for Pt/C catalysts. Reaction conditions: 0.5 mM of NADH in 100 mL of phosphate buffer (0.1 M, pH 7), 0.1 g of catalyst, 30 mL min⁻¹ of N₂ and at 310 K.

Tables

Table 1. Summary of the physicochemical properties of the Pt/C catalysts.

Catalyst	Pt loading (% w/w)	S_{BET} (m² g⁻¹)	Possible main contributing surface groups	Pt particle size range (nm)	Mean Pt particle size (nm)
Pt/C-1	0.85	344	Quinone type carbonyls	1.1-4.3	2.6
Pt/C-2	0.87	478	Carboxylic acids	1.3-4.7	3.2
Pt/C-3	1.07	426	Carboxylic acids	0.8-5.1	2.3
Pt/C-4	0.87	390	Anhydrides, lactones	0.9-7.5	3.9
Pt/C-5	0.66	376	Phenols, anhydrides, lactones	0.7-7.4	2.8
Pt/C-6	0.73	474	Phenolic groups	1.4-9.6	4.6

Table 2. Biocatalytic Alcohol Oxidation with *in situ* NAD⁺ Regeneration using Pt/C-6 Catalyst. ^a

Substrate	Product	Enzyme	Product concentration with Pt/C-6 catalyst (mM)	Conversion (%)	Product concentration without Pt/C-6 catalyst (mM)	Product concentration without enzyme catalyst (mM)
 1-Heptanol	 Heptanal	TesADH	0.13 ± 0.01	6.5	ND ^b	ND ^b
 (S)-(+)-2-Octanol	 2-Octanone	ADH-hT	1.16 ± 0.05	58	ND ^b	ND ^b
 (S)-(-)-1-Phenylethanol	 Acetophenone	AA-ADH	0.35 ± 0.06	18	ND ^b	ND ^b
 1,5-Pentanediol	 δ -Valerolactone	HL-ADH	0.22 ± 0.02	11	ND ^b	ND ^b

^[a] All values correspond to the mean (n=3). Errors correspond to one standard deviation. The reaction system comprised 2 mM substrate, 10 mg mL⁻¹ Pt/C-6 catalyst, 40 μ M NADH and 50 μ g mL⁻¹ enzyme; reaction time: 6 h; except the listed products, no by-products were detected.

^[b] Not detectable.

TOC

